POLITECNICO DI TORINO
Repository ISTITUZIONALE

Status of the NUMEN Construction

Original
Status of the NUMEN Construction / Pierroutsakou, D., Acosta, L., Added, N., Agodi, C., Aguiar, V.A.P., Amador-Valenzuela, P., Anastasio, A., Auerbach, N., Avanzi, L.H., Ayyad, Y., Babu, R., Babu, Y., Bijker, R., Boiano, A., Boztosun, I., Brasolin, S., Brischetto, G.A., Bussa, M.P., Calvo, D., Cappuzzello, F., et al.. - In: EPJ WEB OF CONFERENCES. - ISSN 2100-014X. - ELETTRONICO. - 333:(2025), pp. 1-11. (46th Symposium on Nuclear Physics Cocoyoc, Morelos, México January 6th-9th, 2025) [10.1051/epjconf/202533303006].

Availability:
This version is available at: 11583/3002731 since: 2025-09-02T13:36:55Z

Publisher:
EDP Sciences

Published
DOI:10.1051/epjconf/202533303006

Terms of use:

This article is made available under terms and conditions as specified in the corresponding bibliographic description in the repository

Publisher copyright

(Article begins on next page)

27 November 2026

Status of the NUMEN Construction

D. Pierroutsakou[1,*], *L.* Acosta[2], *N.* Added[3], *C.* Agodi[4], *V.A.P.* Aguiar[3], *P.* Amador-Valenzuela[5], *A.* Anastasio[1], *N.* Auerbach[6], *L.H.* Avanzi[7], *Y.* Ayyad[8], *R.* Babu[9], *Y.* Babu[8], *R.* Bijker[10], *A.* Boiano[1], *I.* Boztosun[11], *S.* Brasolin[12], *G.A.* Brischetto[4], *M.P.* Bussa[12,13], *D.* Calvo[12], *F.* Cappuzzello[14,4], *D.* Carbone[4], *E.N.* Cardozo[15], *G.* Castro[4], *M.* Cavallaro[4], *K.* Challa[12], *E.R.* Chávez Lomelí[2], *E.F.* Chinaglia[7], *I.* Ciraldo[4], *M.* Colonna[4], *A.* Comite[16], *M.* Cortesi[17], *K.M.* Costa[7], *G.* D'Agostino[4], *H.* Dapo[18], *C.* De Benedictis[12,19], *G.* De Gregorio[20,1], *L.M.* Donaldson[21], *F.* Dumitrache[12], *A.* Huerta Hernandez[2], *D.* Gambacurta[4], *E.* M. Gandolfo[22], *H.* Garcia-Tecocoatzi[23], *A.* Gargano[1], *C.* Garofalo[14,4], *M.* Giovannini[16,24], *R.* Gleason[2], *A.* Hacisalihoglu[25], *C.* Ferraresi[12,26], *J.L.* Ferreira[15], *V.* Izzo[1], *S.* Koulouris[27], *Y.* Kucuk[11], *T.C.* Khumalo[21,28], *L.* La Fauci[4], *J.A.* Lay[29], *H.* Lenske[30], *R.* Linares[15], *C.* Lombardo[4], *J.M.* López González[8], *J.* Lubian[15], *D.J.* Marín-Lámbarri[2], *J.* Mas-Ruiz[10], *S.H.* Masunaga[7], *N.H.* Medina[3], *M.* Moralles[31], *L.* Neri[4], *R.* Neveling[21], *Thang* Nguyen[32], *J.R.B.* Oliveira[3], *A.* Pakou[33], *K.* Palli[27,33], *A.* Pandalone[1], *L.* Pandola[4], *R.* Panero[12], *M.* Paterna[12,19], *N.* Pietralla[34], *A.* Pitronaci[4], *L.* Pellegri[21,28], *R.* Persiani[35], *H.* Petrascu[36], *A.* Rovelli[4], *A.D.* Russo[4], *S.* Sandoval-Hipólito[2], *T.M.* Santarelli[7], *E.* Santopinto[24], *R.B.B.* Santos[7], *D.* Sartirana[12], *J.V.* Schervenin[37], *O.* Sgouros[4], *S.O.* Solakcı[11], *V.* Soukeras[4], *G.* Souliotis[27], *A.* Spatafora[4], *D.* Torresi[4], *B.* Urazbekov[38,39], *C.* Valencia[2], *I.* Valinotto[12], *A.* Vanzanella[1], *R.I.M.* Vsevolodovna[24], *A.* Yildirim[11], and *V.A.B.* Zagatto[15]

[1]Istituto Nazionale di Fisica Nucleare, Sezione di Napoli, Napoli, Italy
[2]Instituto de Física, Universidad Nacional Autónoma de México, México City, México
[3]Instituto de Fisica, Universidade de Sao Paulo, Sao Paulo, Brazil
[4]Istituto Nazionale di Fisica Nucleare, Laboratori Nazionali del Sud, Catania, Italy
[5]Instituto Nacional de Investigaciones Nucleares, México
[6]School of Physics and Astronomy, Tel Aviv University, Israel
[7]Centro Universitario FEI, Sao Bernardo do Campo, Brazil
[8]IGFAE, Universidade de Santiago de Compostela, Santiago de Compostela, Spain
[9]Istituto Nazionale di Fisica Nucleare, Sezione di Genova, Italy
[10]Instituto de Ciencias Nucleares, Universidad Nacional Autónoma de México, Mexico
[11]Department of Physics, Akdeniz University, Turkey
[12]Istituto Nazionale di Fisica Nucleare, Sezione di Torino, Torino, Italy
[13]Dipartimento di Fisica, Università di Torino, Italy
[14]Dipartimento di Fisica e Astronomia "Ettore Majorana", Università di Catania, Catania, Italy
[15]Instituto de Fisica, Universidade Federal Fluminense, Brazil
[16]Dipartimento di Chimica e Chimica Industriale, Università di Genova, Italy
[17]Michigan State University, East Lansing, MI, US
[18]Ankara University, Institute of Accelerator Technologies, Turkey
[19]DISAT, Politecnico di Torino, Torino, Italy
[20]University of Campania "Luigi Vanvitelli", Caserta, Italy
[21]iThemba Laboratory for Accelerator Based Sciences, Faure, Cape Town, South Africa
[22]GSI Helmholtzzentrum für Schwerionenforschung GmbH, Darmstadt, Germany
[23]Instituto Tecnológico y de Estudios Superiores de Monterrey, México

[*]dimitra.pierroutsakou@na.infn.it

© The Authors, published by EDP Sciences. This is an open access article distributed under the terms of the Creative Commons Attribution License 4.0 (https://creativecommons.org/licenses/by/4.0/).

[24]Istituto Nazionale di Fisica Nucleare, Sezione di Genova, Genova, Italy
[25]Recep Tayyip Erdogan University, Department of Physics, Turkey
[26]DIMEAS, Politecnico di Torino, Torino, Italy
[27]Department of Chemistry, National and Kapodistrian University of Athens and HINP, Greece
[28]School of Physics, University of the Witwatersrand, Johannesburg, South Africa
[29]Departamento de FAMN, University of Seville, Spain
[30]Department of Physics, University of Giessen, Germany
[31]Instituto de Pesquisas Energeticas e Nucleares, Sao Paulo, Brazil
[32]Florida State University, Florida, US
[33]Department of Physics and HINP, University of Ioannina, Greece
[34]Institut fur Kernphysik, Technische Universitat Darmstadt, Germany
[35]Istituto Nazionale di Fisica Nucleare, Sezione di Catania, Catania, Italy
[36]Department of Nuclear Physics, Horia Hubulei Nat. Inst. Phys. and Nucl. Eng., IFIN-HH, Romania
[37]Instituto de Fisica, Universidade de Sao Paulo, Brazil
[38]Department of Nuclear Physics and Nanotechnology, L. N. Gumilyov Eurasian National University, Astana, Kazakhstan
[39]Institute of Nuclear Physics, Laboratory of Low Energy Reactions, Almaty, Kazakhstan

Abstract.
The NUMEN (NUclear Matrix Elements for Neutrinoless double beta decay) project at INFN-Laboratori Nazionali del Sud aims to extract quantitative information on the Nuclear Matrix Elements relevant to neutrinoless double beta decay, a key process for determining whether the neutrino is a Majorana or Dirac particle and for establishing its effective mass. This objective will be pursued by measuring the cross sections of double charge exchange reactions induced by intense heavy-ion beams on selected isotopes that are candidates for neutrinoless double beta decay. The need to measure extremely low cross sections with high statistical significance has driven a major upgrade of the entire INFN-LNS infrastructure, enabling the production of heavy-ion beams with intensities up to 10^{13} pps at the position of the experimental target. Additionally, significant enhancements are being made to the focal plane detectors of the existing MAGNEX spectrometer. A new target system and advanced detectors are under development to track and identify heavy ions at an expected rate of 5×10^{6} Hz at full beam intensity, while also allowing γ-ray detection. This contribution provides an overview of the current status of the NUMEN project, highlighting recent developments and characterization campaigns for nuclear targets and detector systems.

1 Introduction

Neutrinoless double beta decay ($0\nu\beta\beta$) is a hypothetical isobaric transition in which a parent nucleus (A,Z) transforms into a daughter nucleus (A,Z+2) with the emission of two electrons but no electron antineutrinos. Its observation, which is forbidden by the Standard Model, would provide direct evidence of lepton number violation, with profound implications for our understanding of the Universe's evolution and the matter-antimatter asymmetry. Moreover, it would determine the nature of the neutrino —whether it is a Dirac or Majorana particle— confirming the latter and costrain the effective neutrino mass, provided that the Nuclear Matrix Elements (NMEs) of the involved operators are accurately known. However, current calculations of NMEs, based on various nuclear structure models, exhibit significant uncertainties [1, 2].

Different approaches are being pursued to extract information on $0\nu\beta\beta$ NMEs through experimentally accessible observables. The NUMEN project aims to provide insights into

$0\nu\beta\beta$ NMEs by measuring the cross sections of heavy-ion Double Charge Exchange (DCE) reactions on isotopes that are candidates for $0\nu\beta\beta$ decay [3–5]. DCE reactions involve the exchange of two charge units between the projectile and the target while preserving the initial mass partition. These reactions can occur through sequential nucleon transfer mechanisms, which have been shown to make a negligible contribution [6], or through the exchange of two isovector charged mesons, either in an uncorrelated two-step single charge exchange process [7] —analogous to two-neutrino double beta decay ($2\nu\beta\beta$)— or in a correlated manner between target and projectile. The latter process, known as Majorana DCE, closely resembles $0\nu\beta\beta$ decay [8, 9], suggesting that their NMEs are related [3–5].

The NUMEN project plans to utilize oxygen, neon and carbon beams at energies ranging from 15 to 70 AMeV on several candidate isotopes of interest, including ^{48}Ca, ^{76}Ge, ^{82}Se, ^{100}Mo, ^{124}Sn, ^{128}Te, ^{130}Te, ^{136}Xe, ^{148}Nd, ^{150}Nd, ^{154}Sm, ^{160}Gd, and ^{198}Pt. Examples of DCE reactions relevant to $\beta^-\beta^-$ decay include (^{20}Ne,^{20}O) on ^{116}Cd, ^{130}Te, and ^{76}Ge targets, while those relevant to $\beta^+\beta^+$ decay include (^{18}O,^{18}Ne) on ^{48}Ti, ^{76}Se, and ^{116}Sn targets. The beams are delivered by the Superconducting Cyclotron (CS) at LNS-INFN, and the experiments utilize the large-acceptance MAGNEX magnetic spectrometer [10], equipped with Focal Plane Detectors (FPD) for ejectile detection and the newly developed G-NUMEN array positioned around the target for γ-ray detection.

A pioneering experimental campaign conducted by the NUMEN collaboration demonstrated that precise DCE cross sections can be measured even at very forward angles [11, 12]. The resulting high-resolution spectra in terms of energy, mass, and angular distribution allow for the clear identification of ground-state-to-ground-state transitions of interest [3, 4]. Beyond DCE reactions, simultaneous investigations of other reaction channels will facilitate the evaluation of competing multi-nucleon transfer processes. Moreover, this comprehensive approach will enable a deeper understanding of the reaction mechanisms and a constrained analysis of nuclear states relevant to both DCE reactions and $0\nu\beta\beta$ decay.

However, the DCE cross section represents only a small fraction of the total reaction cross section, making it particularly challenging to study isotopes with extremely low cross sections relevant to $0\nu\beta\beta$ decay. These cases require highly sensitive measurements to distinguish the DCE signal from background noise, which must be minimized. Additionally, cross section measurements must achieve the highest possible statistical significance.

To meet these stringent requirements, a major upgrade of the CS and its associated infrastructure has been undertaken, enabling the delivery of high-intensity beams with intensities two orders of magnitude higher than before. Moreover, an advanced experimental setup for high-sensitivity spectroscopy has been developed, capable of operating in a high-radiation environment. The details of this upgrade are outlined in the Technical Design Report of the NUMEN project and its subsequent updates [13–18].

2 Focal Plane Detectors

The FPD are employed to track the reaction ejectiles and to determine their atomic number (Z), isotopic species (A), and atomic charge state (q) [19]. The limitations of the previous FPD system [20, 21], which consisted of a low-pressure gas drift chamber with proportional wires for primary electron multiplication, followed by a stopping wall of silicon detectors, are mainly related to its maximum operational rate of a few kHz and the limited radiation hardness of the silicon detectors.

The new generation of FPDs is designed to withstand rates of up to 50 kHz/cm, with radiation hardness up to a fluence of 10^{11} ions/cm^2/year. Additionally, it must provide particle identification capabilities for ejectiles with Z $\sim$ 10 and A $\sim$ 20, a time resolution better than 2

ns, a double-hit event probability below 3% across the entire FPD, and the ability to operate in a low-pressure gas environment (tens of mbar).

To fulfill these demanding requirements, a gas tracker has been developed in which the traditional multiplication wires are replaced by Multi-Thick Gas Electron Multiplier foils, followed by a stopping telescope composed of large-area Silicon Carbide (SiC) detectors and Thallium-doped Cesium Iodide [CsI(Tl)] scintillators. Details on the mechanical design, dimensions, and materials of the new FPD system, which is currently under development, are provided in [14, 15, 17, 18]. Here, we summarize its main characteristics and present the results of selected test campaigns conducted to evaluate its performance.

2.1 Gas Tracker

The gas tracker is designed to provide the phase space parameters of the reaction ejectile at the focal plane: $x_{\mathrm{foc}}, y_{\mathrm{foc}}$ with resolution below 0.6 mm, and $\theta_{\mathrm{foc}}, \phi_{\mathrm{foc}}$ with resolution below 5 mrad. High-resolution measurements of these parameters are crucial for accurate particle trajectory reconstruction, allowing the determination of the momentum vector at the target position and, consequently, the particle scattering angle and energy.

The adopted solution consists of a proportional drift chamber with a sensitive volume of $1200\times116\times108$ mm^3, equipped with a thin Mylar entrance window and filled with isobutane gas. The electron multiplication stage is based on a three-layer Thick Gas Electron Multiplier (M-THGEM), where each layer consists of an insulating plane sandwiched between two conductive layers with a high density of microscopic holes, manufactured using a multilayer PCB technique (total thickness about 1 mm). Primary electrons, generated along the ion track, drift under a uniform electric field toward the M-THGEM, where they undergo avalanche multiplication due to the high field. The resulting avalanche electrons are collected on a segmented anode, while the bottom electrode of the M-THGEM collects the positive ions. The charge distribution on the segmented anode provides the horizontal position (x, z) and the track angle θ, while the vertical position y and the angle ϕ are derived from the electron drift time.

To optimize the gas tracker performance, different M-THGEM hole geometries, coupled with strip- and pad-segmented anodes, were tested on the first gas tracker prototype. The characterization was carried out by measuring the currents flowing through the electrodes, employing a picoammeter with 7 ADC channels (15 pA precision, 10 mV sensitivity), as a function of the applied voltages, gas pressure, and incident particle rate. These tests were done using α sources and ^{18}O ions at E = 270 MeV at the INFN-LNS Test Bench [22]. The results demonstrated that high gas gains of $\sim 10^5$ can be achieved even at low pressures ($\sim$ 10 mbar) with minimal ion backflow (IBF). The IBF, defined as the fraction of positive ions collected on the cathode relative to the total charge, is a critical parameter since excessive ion backflow can distort the electric field in the drift region, degrading position resolution and drift time measurements.

The best performance was obtained using a full-coverage THGEM foil configuration with holes arranged in a square pattern, coupled with an anode segmented into pads in the x-z plane, five rows along z, each with 60 pads in the x direction, as shown in **Figure 1A, B**. Based on these findings, a second prototype was developed featuring the above M-THGEM and anode design but scaled to one-fourth of the full tracker length along the dispersive x-direction (**Figure 1C**). The position resolution of the prototype was assessed using a collimated α source, yielding a preliminary FWHM resolution in the x-direction of less than 1 mm.

The prototype (**Figure 1C**) was recently tested at the Pelletron facility of the Institute of Physics, University of São Paulo, Brazil. This experiment aimed to simulate the NUMEN beam conditions in terms of energy loss within a low-pressure gas volume. The following beams were used: (i) ^{12}C at 45 MeV and 37.5 MeV and (ii) ^{7}Li at 32 MeV and 28 MeV. The

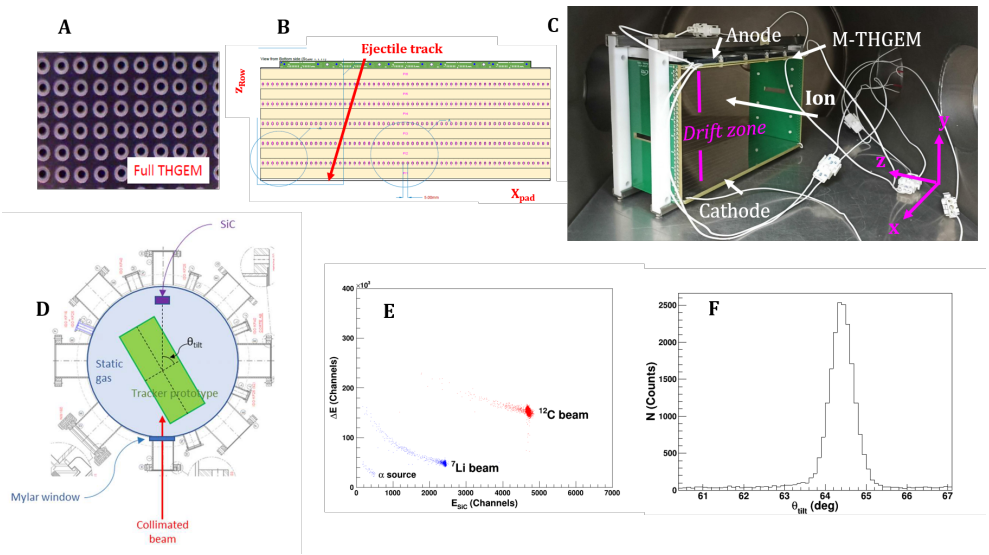

Figure 1. (A) Small area of the Full THGEM foil configuration. (B) Pad-segmented anode: 5 rows (z-direction), each with 60 pads in the dispersive x-direction. (C) Gas tracker prototype with the M-THGEM and anode shown in the same figure. (D) Schematic experimental setup. (E) Online bidimensional plot ΔE-E_{SiC} from the gas tracker prototype and the SiC detector. (F) Online reconstructed tilt angle θ_{tilt}.

experiment was carried out at the SAFIIRA facility, located at the 0° beamline, which is optimized for delivering high-quality beams into a multipurpose scattering chamber [23]. The beams were well-collimated (0.3 mm diameter, 0.2° FWHM divergence) and their intensity was carefully controlled (ranging from 10 Hz to 3 kHz). A schematic of the experimental setup is presented in **Figure 1D**. The accelerated beam passed through a thin Mylar window at the entrance of the 45 cm-diameter scattering chamber, filled with high-purity (99.95%) isobutane gas. The chamber pressure was varied across different runs. The tracker prototype was mounted inside the chamber at a tilt angle θ_{tilt}, which was varied from 40° to 60° in order to explore different ion trajectories. A SiC detector was placed downstream to stop the beam and provide a timing reference for measuring the electron drift time. During the experiment, the following aspects were investigated: (i) Tracker position and angular resolution; (ii) Dependence of performance on θ_{tilt} and (iii) Tracker response to beam rate variations. Data analysis is currently in progress, and results will be presented in a forthcoming publication. **Figure 1E** shows an online bidimensional spectrum of ΔE in the gas tracker *vs*. residual energy E_{SiC} in the SiC detector, while **Figure 1F** presents the online reconstruction of the tilt angle θ_{tilt}.

2.2 Particle Identification Wall

The particle identification (PID) is carried out by combining the measurement of the horizontal position x_{foc} at the focal plane, provided by the gas tracker, with the energy loss (ΔE) and residual energy (E_r) of the incident ions, detected by a dedicated array of 720 SiC-CsI(Tl) telescopes. These telescopes are arranged in 36 towers, each tilted by approximately 35° with respect to the vertical axis to partially compensate for the inclination of the focal plane relative to the optical axis of the MAGNEX dipole magnet.

Each SiC element has an active area of 1.5×1.5 cm^2, with a peripheral edge structure of 0.4 mm width, a thickness of 100 μm, and a 10 μm-thick dead layer on the back side. The

CsI(Tl) inorganic scintillator is 5 mm thick and is coupled to a Hamamatsu S3590 photodiode with an active area of 1×1 cm^2.

The first prototypes of such large-area SiC detectors were fabricated using epitaxial silicon carbide growth with two different doping concentrations, namely, 3×10^{13} atm/cm^3 and 9×10^{13} atm/cm^3, corresponding to different depletion voltages. These detectors were developed as part of the NUMEN R&D program to design a new PID Wall for the MAGNEX FPD. This marked the first time that SiC detectors with such a large area ($\sim$ 2.4 cm^2) and a thick epitaxial layer ($\sim$ 100 μm) were produced and characterized [24]. Doping concentration plays a critical role in the development of SiC detectors for NUMEN, as they must operate in a low-pressure environment. This requirement imposes a low depletion voltage to prevent discharge effects, necessitating a lower doping concentration than the conventional 10^{14} atm/cm^3.

To determine the full depletion voltage and doping profile of the SiC detectors, current-voltage and capacitance-voltage characteristics were investigated. Energy resolution and depletion depth were evaluated using radioactive α-sources. The tested detectors exhibited a good energy resolution ($\sim$ 0.5% FWHM), well within the NUMEN requirement of $\leq$ 2%. However, differences in depletion depth and doping profile were observed between detectors from the two wafers. The low-doping wafer exhibited a depletion depth lower than the nominal value and a poorer performance in terms of the doping profile.

Since a lower doping concentration is essential for NUMEN, new wafers were recently produced using a different doping process. The obtained doping profiles appear to meet the required uniformity standards, and further tests will be conducted once detector fabrication is completed.

Regarding radiation hardness, the PID Wall components have demonstrated excellent resistance to ionizing radiation. The SiC detectors have withstood fluences up to 10^{13} ions/cm^2 [14, 25, 26], while the CsI(Tl) scintillators have endured fluences exceeding 7.5×10^{11} ions/cm^2 [14], fully satisfying the NUMEN experiment requirements.

A test campaign was undertaken at the TANDEM+ALPI facility of INFN-LNL to evaluate the PID Wall's Z-identification capability, response to high rates and sensitivity to the tilt angle. A ^{16}O beam at 15 AMeV was used, with two PID Wall towers placed at forward angles inside the PISOLO scattering chamber. Preliminary results indicate: Z-resolution $\Delta Z/Z \sim 1/34$ and mass resolution $\Delta A/A \sim 1/47$, ensuring unambiguous particle identification; excellent time resolution in the order of hundreds of ps for the SiC detectors and double-hit probability below 2.5%, demonstrating the effectiveness of the chosen segmentation. Data analysis is ongoing, and the final results will be presented in a forthcoming publication.

Additional research on SiC sensors has recently been carried out at the Ruđer Bošković Institute, Zagreb. The focus of this study was to investigate the charge collection efficiency (CCE) across the entire active volume and near the detector edges, a crucial aspect for guaranteeing uniform response. This investigation was performed using the Ion Beam-Induced Charge technique, which employs focused MeV-range accelerated ions with a beam spot as small as $\sim$ 1μm to probe charge transport within the detector. Preliminary results show excellent uniformity in the central region of the SiC sensors, where the CCE remains constant and a noticeable decrease in CCE near the sensor boundaries, where CCE tends to drop to zero. These findings are crucial for optimizing the detector design and ensuring a consistent response over the entire active area.

3 The G-NUMEN γ spectrometer array

DCE events can be detected with high selectivity using the MAGNEX spectrometer [27, 28], which provides an energy resolution of approximately 500 keV at low incident energy. This resolution is sufficient to distinguish the ground state from the first excited state for non-deformed nuclei in both projectile and target. However, for deformed target nuclei such as ^{110}Pd, ^{150}Nd, and ^{160}Gd, as well as for cases involving high incident energies, this resolution is inadequate. To address this limitation, the G-NUMEN γ-ray spectrometer was introduced around the target position. This system detects γ-rays in coincidence (or anti-coincidence) with projectile-like fragments in the FPD, allowing the discrimination of closely spaced energy states [13, 29]. G-NUMEN consists of 110 $LaBr_3$(Ce) scintillators coupled with Hamamatsu R6231 8-dynode-stage photomultiplier tubes (PMTs), with the entire detector system supplied by EPIC Crystal (EPIC from now on). Each crystal has a diameter of 38 mm and a length of 50 mm. Positioned 24 cm from the target, the detectors cover a solid angle of 20% and exhibit an expected total photopeak efficiency of 4% at 1.3 MeV.

The main requirements for the G-NUMEN detectors are [13]: (i) a time resolution of a few ns to differentiate between consecutive beam bunches and suppress random coincidence backgrounds; (ii) an energy resolution better than 10% at 200 keV; (iii) a low observational limit; (iv) stable PMT charge conversion gain (defined as the ratio of output pulse charge to incident photon energy) at count rates up to ~300 kHz; (v) a linear response of output pulse charge to incident photon energy and (vi) radiation hardness to fast neutrons up to 10^{11} neutrons/cm^2, the expected neutron fluence in a 1-month long experiment as estimated from FLUKA simulations [30].

The G-NUMEN detectors were tested under various count-rate conditions, replicating those expected in NUMEN experiments. The high count-rate tests involved the use of intense radioactive sources, a laser system delivering light to the PMT via an optical fiber, and a fusion-evaporation experiment conducted at the ALTO facility of the IJC Laboratory [31]. The results revealed that detector performance is influenced by count rate, high voltage (HV), and the electronic configuration of the PMT voltage divider.

Using the EPIC active voltage divider, the PMT charge conversion gain exhibited a dependence on the count rate, with the output signal degrading beyond a critical threshold that varied with the applied HV. This threshold defined the maximum sustainable count rate for the detector, which remained well within the operational range required for the NUMEN experiments. The percent variation of the PMT gain as a function of count rate at various HVs is presented in Figure 2A, where the limiting rate is identified as the point at which the gain undergoes a sudden increase. Furthermore, low-rate measurements showed that the charge of the output pulse deviated from linearity as the incident photon energy increased, with this effect becoming more pronounced at higher HV levels (Figure 2B).

To resolve these issues, a new active voltage divider was developed by the NUMEN collaboration, employing PMOS transistors to stabilize interstage voltages of the PMT dynodes. This configuration eliminates gain variation and count-rate limitations. Furthermore, optimizing the voltage gradient across dynodes (a "tapered" voltage divider) improves pulse linearity. With this new voltage divider a highly stable gain (within 0.5% across the full range), excellent energy resolution (2.8% FWHM at 662 keV, 6.4% at 122 keV), sub-ns timing resolution and an improved linearity with energy were achieved, fully meeting NUMEN requirements (figures 2D, E). A forthcoming paper will present a detailed analysis of these results.

A crucial experiment was performed at the ALTO facility (IJCLab, Orsay) to verify the capability of G-NUMEN (in coincidence with MAGNEX) to distinguish γ-rays from DCE events amidst intense backgrounds from projectile-target interactions. A ^{16}O beam at 83.5 MeV was directed onto a Ti target, followed by a Ta target. The experiment replicated the

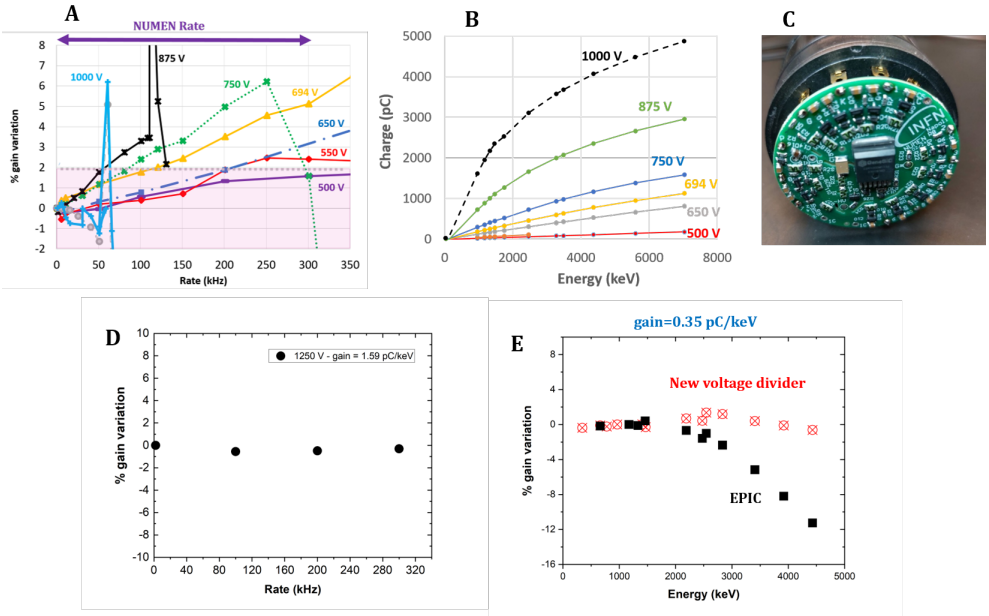

Figure 2. With the EPIC active voltage divider at various HVs (A) Percent variation of the charge conversion gain (normalized to the gain at low rate) *vs* count rate and (B) Charge of the output pulse *vs* incident photon energy (C) The newly developed active voltage divider (D) the same quantities shown in A for the new active voltage divider at HV=1250 V (E) percent variation of the charge conversion gain (normalized to the gain at low energy) *vs* incident photon energy with the two voltage dividers at the same gain, 0.35 pC/keV. The corresponding HVs are: 755 V for EPIC and 780 V for the new voltage divider.

signal-to-background ratio of a NUMEN experiment with a 10^{12} pps beam intensity. Preliminary results are consistent with previous GEANT simulations [13, 32], confirming that particle-γ coincidence allows for effective signal discrimination when high trigger selectivity is ensured, as in the case of MAGNEX for the NUMEN experiments. A complete analysis of the results will be presented in an upcoming publication.

While $LaBr_3(Ce)$ scintillators are expected to be radiation-hard to fast neutrons, previous studies were limited to fluences of 10^8 neutrons/cm^2—three orders of magnitude below NUMEN requirements. To extend this study, the NUMEN collaboration carried out an experiment at the ALTO facility, exposing detectors to fluences up to 10^{10} neutrons/cm^2 using the LICORNE neutron source that provides fast neutrons (with energy up to 3 MeV) via the ^{7}Li(p,n)^{7}Be reaction at 16.7 MeV in inverse kinematics [33]. Measurements before, during, and after neutron exposure assessed changes in intrinsic background, time resolution, gain, and energy resolution. Preliminary results indicate an increased intrinsic background post-irradiation, with full recovery after one week. The light yield decreased by 4%, stabilizing at a 3% reduction after one week. The energy resolution degraded by 5% but fully recovered within 20 days, while the time resolution remained unaffected. These findings suggest that $LaBr_3(Ce)$ meets NUMEN requirements up to 10^{10} neutrons/cm^2, though continuous energy calibration is needed to correct light yield variations. Future tests will explore neutron fluences up to 10^{11}-10^{12} neutrons/cm^2.

4 Target system

One of the most challenging aspects of the R&D activities within the NUMEN project concerns the production of targets composed of specific isotopes, which must be irradiated with intense ion beams while ensuring high energy resolution of the reaction products and allowing the collection of sufficient statistics for DCE reactions.

This can be achieved by depositing a few hundred nanometers of isotopic material onto high thermal conductivity backings characterized by low stopping power, high mechanical strength, high purity, and minimal thickness. Suitable substrates include graphite foils such as Highly Oriented Pyrolytic Graphite (HOPG) or alternative multi-layer graphene (MLG) candidates. These materials exhibit high in-plane thermal conductivity, enabling efficient heat dissipation to a cooled frame that acts as the mechanical support for the target. The developed cooling system consists of a target encased in a copper holder, mounted on top of a cryocooler capable of dissipating up to 20 W while maintaining a temperature of 40 K. Due to the high-radiation environment at the target position, an automated system was necessary to handle the replacement of irradiated targets and their storage, eliminating the need for human intervention. A detailed description of the entire target system and its automated handling is provided in [17, 18].

Initial target production attempts utilized HOPG substrates (supplied by Optigraph, Germany). These first depositions were performed using electron-beam evaporation of Ge, Te, Se, Mo, Sn, and Cd isotopes, varying the evaporation rate, modifying the thickness and temperature of the HOPG substrate, and, in some cases, employing a deposition buffer to enhance the diffusion of evaporated material onto the backing surface. To characterize the target and substrate properties, various analytical techniques were employed, including: (i) Transmission of α-particles from a radioactive source through the sample, followed by their detection using a 100 μm-thick silicon detector to assess thickness and non-uniformity (APT method); (ii) Scanning Electron Microscopy (SEM) to investigate surface morphology with nanometer-scale resolution in the planar axes and (iii) Rutherford Backscattering Spectroscopy (RBS) at INFN-LNL, using proton and α-particle beams to evaluate thickness and conduct elemental analysis of both target and substrate.

Target production proved to be highly complex due to the stringent requirements for low thickness and high uniformity, which are essential for preserving good energy resolution. For isotopes such as Ge and Te, the best results were obtained under standard evaporation conditions, i.e., without substrate heating, without a deposition buffer, and at a low evaporation rate (0.2–0.5 Å/s) [34]. However, successful Mo target depositions were achieved via electron-beam evaporation onto HOPG backings at a substrate temperature of 300°C, yielding excellent Mo adhesion [35]. For this isotope, substrate heating was found to be crucial in mitigating post-evaporation stresses and preventing delamination effects, which typically lead to significant non-uniformities on the target surface.

An important aspect of target R&D involves investigating radiation damage to the substrate, particularly the formation of defects such as atomic dislocations, vacancies, and broken chemical bonds. Understanding these degradation mechanisms helps to determine the replacement frequency of target-substrate systems during experiments, as crystalline defects impair the substrate's thermal conductivity. To evaluate radiation damage, HOPG foils were irradiated with monoenergetic 14 MeV neutrons from a Deuterium-Tritium neutron generator at the Instituto de Estudos Avançados (IEAv) in São José dos Campos, Brazil, to fluences of 1.7×10^{10} neutrons/cm^2. Structural analyses revealed a 50% reduction in thermal conductivity due to neutron-induced crystal defects. Morphological and crystallographic characterizations were performed using X-ray diffraction (XRD), micro-Raman spectroscopy, Atomic Force Microscopy, and SEM [36]. Simulations of 14 MeV neutron interactions with ^{12}C demon-

strated that crystalline damage results from multiple physical mechanisms, including atomic displacement and energy transfer to both the crystalline lattice and ionization of HOPG. The dominant contribution to the damage stems from the interaction of α particles, produced in the ^{12}C(n,α)^{9}Be channel.

To evaluate the energy resolution (ΔE) of the first target prototypes, analytical calculations were carried out for ejectiles detected at 0° relative to the incident beam in the ^{130}Te(^{20}Ne,^{20}O)^{130}Xe DCE reaction at 15 AMeV. The analysis considered various contributing factors, including beam energy spread, the intrinsic resolution of the MAGNEX spectrometer, and target-substrate effects [34]. It was found that the non-uniformity of the HOPG substrate was the dominant contribution to ΔE. To ensure sufficient separation between the ground and first excited states of ^{130}Xe, the substrate's non-uniformity should be $\leq$10%. However, multiple HOPG samples exhibited higher non-uniformity, rendering them unsuitable as substrates for NUMEN targets.

Given the limitations of HOPG, current R&D efforts focus on exploring MLG foils as alternative target substrates. Various MLG samples, produced by different methods and sourced from multiple companies (Kaneka, ACF-metals, Nanotech, Micromatter), are being evaluated and characterized. Their thermal conductivity is estimated from the density, through XRD measurements, and literature-reported thermal diffusivity values. Thickness and non-uniformity are measured using APT, while radiation damage is investigated via Raman spectroscopy to examine defects in the graphene structure. Additionally, new synthesis techniques for MLG foils are being explored, including low-pressure filtration and pyrolysis of Kapton. The ultimate goal is to develop materials with tailored structural properties (e.g., high order, smooth surface, layered morphology, thermal stability) suitable for various applications, including NUMEN targets.

For NUMEN-relevant Xe and Kr targets, producing thin samples is particularly challenging due to their inability to form solid compounds. Initial implantation tests were conducted at IFUNAM (Mexico) using electromagnetically selected ^{127}I and ^{81}Br ions implanted into a 50 μm-thick graphite substrate at energies near 1 MeV (200–300 nm depth) [37]. These ions were chosen due to their similarity to noble gases. Post-implantation characterization was obtained via RBS using ^{1}H, ^{12}C, and ^{28}Si beams at various energies and scattering angles. The same methodology will be applied to produce noble gas-implanted Xe and Kr targets in future studies.

5 Conclusions

The NUMEN project pursues an ambitious program focused on the study of DCE reactions. Its primary goal is to precisely measure DCE cross sections at very forward angles, with the hope of gaining insights into the NMEs involved in $0\nu\beta\beta$ decay, which would be crucial for determining the effective neutrino mass should such a decay be observed.

Achieving an accurate measurement of DCE cross sections, which represent only a small fraction of the total reaction cross sections, has required an extensive upgrade of the CS at INFN-LNS and the MAGNEX spectrometer. This is essential for investigating all nuclear candidates for $0\nu\beta\beta$ decay. In particular, significant technological advancements have been necessary for the production of thin, highly uniform targets and substrates capable of withstanding intense ion beam irradiation. New substrate materials are currently being evaluated and characterized using various analytical techniques. Furthermore, considerable efforts have been dedicated to the development of advanced detectors and specialized electronics designed to operate in high-radiation environments.

The construction of the NUMEN experimental setup is at an advanced stage. Several campaigns aimed at characterizing the detectors and targets, as well as assessing their ra-

diation hardness, have been successfully completed, while others are currently in progress. These efforts are crucial to preparing for the project's final phase—commissioning and the start of experimental runs.

References

[1] J. Engel and J. Menendez, Rep. Progr. Phys. **80** 046301 (2017)
[2] A. Belley, T. Miyagi, S. R. Stroberg, and J. D. Holt arXiv:2307.15156v1
[3] F. Cappuzzello et al., Eur. Phys. J. A **51** 145 (2015)
[4] F. Capuzzello et al., Eur. Phys. J. A **54** 72 (2018)
[5] F. Cappuzzello et al, Progr. in Part. and Nucl. Phys. **128** 103999 (2023)
[6] J.L. Ferreira et al., Phys. Rev. C **105** 014630 (2022)
[7] J. I. Bellone et al., Physics Letters B **807** 135528 (2020)
[8] H. Lenske, F. Cappuzzello, M. Cavallaro, M. Colonna, Prog. Part. and Nucl. Phys. **109** 103716 (2019)
[9] H. Lenske, J. Bellone, M. Colonna and D. Gambacurta, Universe **2024** 10, 202
[10] F. Cappuzzello, C. Agodi, D. Carbone and M. Cavallaro, Eur. Phys. J. A **52** 167 (2016)
[11] V. Soukeras et al., Results in Physics **28** 104691 (2021)
[12] C. Eke at al., Results in Physics **67** 108037 (2024)
[13] F. Cappuzzello et al., The NUMEN technical design report, Int. J. Modern Phy. A **Vol. 36** No.30 2130018 (2021)
[14] P. Finocchiaro et al., Universe **2020**, 6, 129
[15] F. Cappuzzello et al. Frontiers in Astronomy and Space Sciences, V.**8** 668587 (2021)
[16] C. Agodi et al., Universe **2021**, 7, 72
[17] D. Calvo et al., Journal of Physics: Conf. Ser. **2374** 012029 (2022) IOP Publishing
[18] D. Calvo et al., Nucl. Inst. Method in Phys. Res. A **1041** 167336 (2022)
[19] F. Cappuzzello et al., Nucl. Inst. Method in Phys. Res. A **621** 419 (2010)
[20] M. Cavallaro et al., Eur. Phys. J. A **48:59** (2012)
[21] D. Torresi et al., Nucl. Inst. Method in Phys. Res. A **989** 164918 (2021)
[22] I. Ciraldo et al., Nucl. Inst. Method in Phys. Res. A **1048** 167893 (2023)
[23] V.A.P. Aguiar et al., Rev. Sci. Instrum. **91** 053301 (2020)
[24] D. Carbone et al., Nucl. Inst. Method in Phys. Res. A **1069** 169960 (2024)
[25] S. Tudisco et al., Sensors **2018**, 18 2289
[26] C. Altana et al., Sensors **2023**, 23(14), 6522
[27] S. Calabrese et al., Nucl. Inst. Method in Phys. Res. A **980** 164500 (2020)
[28] M. Cavallaro et al., Nucl. Inst. Method in Phys. Res. B **463** 334 (2020)
[29] J.R.B. Oliveira et al., J. Phys. Conf. Ser. **1056**:012040 (2018)
[30] T. T. Böhlen, F. Cerutti, M. P. W. Chin et al., Nucl. Data Sheets **120** 211 (2014)
[31] E. M. Gandolfo et al., Instruments **2023**, 7, 28
[32] J.R.B. Oliveira et al., Eur. Phys. J. A **56** 153 (2020)
[33] E.M. Gandolfo, Ph. D. Thesis **2022**, Dip. Fisica "Ettore Pancini", Univ. di Napoli Federico II, Napoli, Italy
[34] M. Fisichella et al., Eur. Phys. J. Web of Conferences **285** 01001 (2023)
[35] M. Fisichella et al., to be published
[36] M.A. Guazzelli et al., Diamond & Related Materials **151** 111803 (2024)
[37] S. Sandoval-Hipólito et al., Nucl. Inst. Method in Phys. Res. B **555** 165485 (2024)